Bifurcation analysis of torsional micromirror actuated by electrostatic forces

M. TAGHIZADEH[1)], H. MOBKI[2)]

[1)] *Department of Mechanical Engineering*
Amirkabir University of Technology
Tehran, Iran
e-mail: taghizadehm@aut.ac.ir

[2)] *Department of Mechanical Engineering*
University of Tabriz
Tabriz, Iran
e-mail: hamedmobki@Live.com

In this paper, static and dynamic behavior of an electrostatically actuated torsional micro-actuator is studied. The microactuator is composed of a micromirror and two torsional beams, which are excited with two electrodes. Unlike in the traditional microactuators, the electrostatic force is exerted to both sides of micromirror, so the model is exposed to a DC voltage applied from the ground electrodes. The static governing equation of the torsional microactuator is derived and the relation between rotation angle and the driving voltage is determined. Local and global bifurcation analysis is performed, considering torsional characteristics of the micro-beams. By solving static deflection equation, the fixed points of the actuator are obtained. Critical values of the applied voltage leading to qualitative changes in the microactuator behavior through a saddle-node or pitchfork bifurcations for different spatial condition are obtained. Furthermore, the effects of different gap and electrode sizes as well as beam lengths on the dynamic behavior are investigated. It is shown that an increase of the applied voltage leads the structure to an unstable condition by undergoing saddle-node and pitchfork bifurcations when the voltages ratio is zero and one, respectively.

Key words: MEMS, torsional actuator, pull-in, pitchfork bifurcation, saddle-node bifurcation.

1. Introduction

Torsional microactuator devices have broad applications in the microelectromechanical systems (MEMS), such as torsional radio frequency (RF) switches, tunable torsional capacitors, digital light processing (DLP) chip, etc. [1–7]. Advances in micromirror technology have enabled the designers to develop the micromechanical sensors, actuators, devices and systems, such as pressure sensors, biological sensors, mirror arrays for high performance projec-

tion displays and other devices [8]. Micromirrors may be classified into four categories based on their motion: deformable micromirror, movable micromirror, piston micromirror, and torsional micromirror [9]. These four types of micromirrors have been extensively applied in recent years [10–13]; however, the torsional micromirrors are the most interesting because they have some advantages, such as good dynamic response and small possibility of adhesion [9].

There are number of common actuation methods in MEMS, which include electrothermal, electromagnetic, piezoelectric and electrostatic. Among these actuation methods, electrostatic actuation is considered to be the most common in MEMS because of its simplicity and high efficiency [14].

One of the most significant topics in the electrostatically actuated micromirrors is the pull-in instability. In such devices, a conductive flexible plate is suspended over a ground and the electrostatic voltage is applied between them. As the micromirror is balanced between electrostatic attractive and mechanical (elastic) restoring torque, both the electrostatic and when the applied voltage is increased the elastic restoring torque are raised. When the voltage reaches a critical value, pull-in instability occurs. Pull-in is a state at which the elastic restoring torque can no longer balance the electrostatic torque [15].

The static and dynamic instabilities of a torsional MEMS/NEMS (nanoelectromechanical systems) actuator caused by capillary effects were studied by Guo et al. [16].

It is common in MEMS to note that the static and dynamic behavior of a system indicates a qualitative change in the features of the system when adjusting one of its control parameters, such as a bias voltage. In nonlinear dynamics, this phenomenon is called bifurcation [14]. Bifurcation analysis of an electrostatic torsional micromirror is essential for making the electrostatic actuation more effective and has been reported in [9, 17–19].

Zhang et al. [9] described the static characteristics of an electrostatically actuated torsional micromirror based on the parallel-plate capacitor model. Degani et al. [17] have studied pull-in analysis for an electrostatically torsional microactuator. Fabrication of microactuators is one of the most accurate and important aspects of studying of a microactuators' behavior. They fabricated two types of microactuators by using bulk micromachining. Jian-Gang and Zhao [18] have studied the influence of van der Waals and Casimir forces on the stability of the electrostatic torsional nanoactuators. Rezazadeh et al. [19] have investigated the electromechanical behavior of a torsional micromirror using a static model of micro-beams. They derived a set of nonlinear equations based on the parallel plate capacitor model to represent the relationships between the applied voltage, torsion angle and vertical displacement of the torsional micromirror.

The influences of Casimir and van der Waals forces on the electrostatic torsional NEMS varactor are studied by Lin and Zhao [20]. They also studied the

Casimir forces effect on the critical pull-in gap and pull-in voltage of nanoelectromechanical switches [21].

In spite of many researches accomplished in the field of static and dynamic behavior of torsional micromirrors, there is not enough study explaining their stability from bifurcation view point. Therefore, this paper is a case study that considers a micromirror suspended over two conductive electrodes actuated by two electrostatic forces. The micromirror is actuated by two electrostatic forces by applying two DC polarization voltages. The dynamic motion equation of the proposed actuator is derived. Fixed points of the micromirror actuator are obtained by solving the static deflection equation. Relative results are illustrated in the state-control space. In order to study the global stability of the fixed points, dynamic responses of actuator are illustrated in phase portraits.

2. Model description

Figure 1 shows schematic 3D view of the torsional microactuator. As shown in this figure, micromirror plate is suspended by two similar torsion beams with length l, width w, thickness t and shear modulus G. The micromirror plate has a length b, width $2L$ and thickness t. There are two stationary electrodes on the substrate beneath the micromirror. Figure 2 presents the cross-section view of the actuator considering torsion effect. As shown in this figure, the micromirror plate distance from the stationary electrode is G_0. The applied voltages between micromirror and the ground electrodes are V_1 and V_2. In order to model the electrostatic torque, it is assumed that the plates are infinitely wide, so fringing fields (fields at the edges of the plates) may be neglected, the deformation of the micromirror plate is very small, and the vertical displacement of the micromirror is mainly attributed to the deflection of the microbeams [22]. Hence,
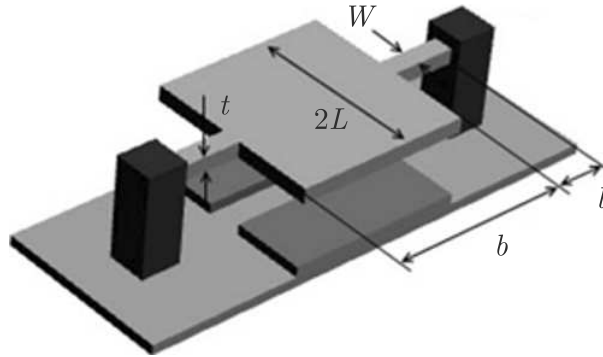

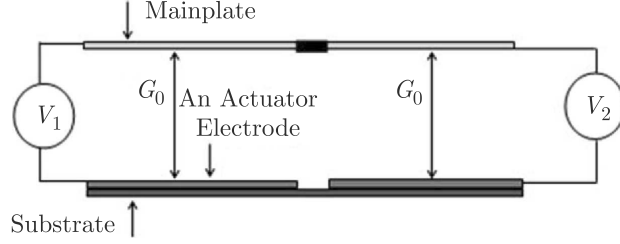Fig. 1. Schematic 3D view of the torsional micromirror.

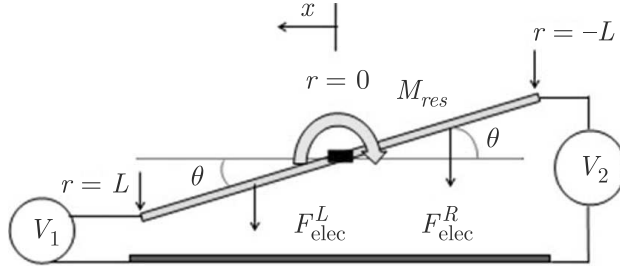Fig. 2. Schematic side view of the torsional actuator.

Fig. 3. One-DOF model of torsional actuator with electrostatic forces.

the micromirror can be modeled as a rigid body with one degree of freedom θ. This parameter is the torsion angle of the beams about z axis, (see Fig. 3). When a voltage between one of the ground electrodes and the micromirror is applied, an electrostatic attracting force between them will produce an electrostatic torque, which is tilted micromirror.

3. Mathematical modeling

The stored electrical energy (W) in a parallel plate capacitor (C) with plate area (A) is given by [8]

$$(3.1) \qquad W = -\frac{1}{2}CV^2 = -\frac{1}{2}\frac{\varepsilon_r \varepsilon A V^2}{u},$$

where u is the distance between the electrodes, ε_r is the relative permittivity of the dielectric material (for air it is about $\varepsilon_r = 1$), and ε is the permittivity of vacuum ($\varepsilon = 8.85 \times 10^{-12} c^2 N^{-1} m^{-2}$). Taking the derivative of W with respect to u yields the electric force between the plates

$$(3.2) \qquad F_{\text{elec}} = \frac{dW}{du} = \frac{1}{2}\frac{\varepsilon A V^2}{u^2}.$$

3.1. Calculations for the left and right electrodes

It is assumed that the effective area of the plate is A, and for an element $dA = bdx$, the distance between the rotational plate element and left and right electrode is $u_1 = G_0 - x\theta$ and $u_2 = G_0 + x\theta$, respectively. Hence, the electrostatic force of a differential element for the left and right side of the micromirror can be written as

$$(3.3) \qquad W_1 = -\frac{1}{2}CV_1^2 = -\frac{1}{2}\frac{\varepsilon A V_1^2}{u_1},$$

$$(3.4) \qquad W_2 = -\frac{1}{2}CV_2^2 = -\frac{1}{2}\frac{\varepsilon A V_2^2}{u_2}.$$

Electrostatic force for left and right side of the micromirror may be obtained by taking the derivative of W_1 with respect to u_1 and W_2 with respect to u_2:

$$(3.5) \qquad F_{\text{elec}}^L = \frac{dW_1}{du_1} = \frac{1}{2}\frac{\varepsilon A V_1^2}{u_1^2},$$

$$(3.6) \qquad F_{\text{elec}}^R = \frac{dW_2}{du_2} = \frac{1}{2}\frac{\varepsilon A V_2^2}{u_2^2}.$$

Thus, the electric force of a differential element can be written as [8]

$$(3.7) \qquad dF_{\text{elec}}^L = \frac{b\varepsilon V_1^2}{2u_1^2}dx,$$

$$(3.8) \qquad dF_{\text{elec}}^R = \frac{b\varepsilon V_2^2}{2u_2^2}dx.$$

The total electrostatic torque of the left and right electrodes about rotation axis is given by integrating contributions of all the plate elements:

$$(3.9) \qquad M_{\text{elec}}^L = \int_0^L x\, dF_{\text{elec}}^L,$$

$$(3.10) \qquad M_{\text{elec}}^R = \int_0^L x\, dF_{\text{elec}}^R.$$

Hence, the left and right electrostatic torques can be written as

$$(3.11) \qquad M_{\text{elec}}^L = \frac{b\varepsilon V_1^2}{2\theta^2}\left[\frac{G_0}{G_0 - L\theta} - 1 + \ln\frac{G_0 - L\theta}{G_0}\right],$$

$$(3.12) \qquad M_{\text{elec}}^R = \frac{b\varepsilon V_2^2}{2\theta^2}\left[\frac{G_0}{G_0 + L\theta} - 1 + \ln\frac{G_0 + L\theta}{G_0}\right].$$

3.2. The equation of motion

The directions of the left and right electrostatic torque are opposite to each other, so the restoring torque, shown in Fig. 3, can be obtained as

$$(3.13) \qquad M_{\mathrm{elec}} = M_{\mathrm{elec}}^{L} - M_{\mathrm{elec}}^{R}.$$

Then, the equation of motion is

$$(3.14) \qquad I\frac{d^2\theta}{dt^2} + \overline{\mu_\theta}\frac{d\theta}{dt} + K_\theta\theta = M_{\mathrm{elec}},$$

where $\overline{\mu_\theta}$ is the damping torque coefficient.

The micromirror plate is suspended by two beams and therefore is subjected to a mechanical torque opposing the electrostatic torque. The beams' mechanical elastic torque can be written as $M_{\mathrm{res}} = K_\theta\theta$, where K_θ is the effective torsion stiffness of the microbeams and is defined for the elastic ranges of deflection as follows [23]:

$$(3.15) \qquad K_\theta = \frac{2c_2wt^3G}{l}.$$

The coefficient c_2 depends on the ratio (w/t). By introducing dimensionless variables [24] we obtain

$$(3.16) \qquad \gamma = \frac{\theta}{\theta_{\mathrm{Max}}}, \qquad p = \frac{V_2}{V_1}, \qquad \tau = \frac{t}{T_\theta}, \qquad \mu_\theta = \frac{\overline{\mu_\theta}}{K_\theta T_\theta}$$

and the characteristic time

$$(3.17) \qquad T_\theta = \sqrt{\frac{I}{K_\theta}}.$$

Equation (3.14) can be transformed into the dimensionless form as follows:

$$(3.18) \qquad \frac{d^2\gamma}{d\tau^2} + \mu_\theta\frac{d\gamma}{d\tau} + \gamma = \frac{\delta V_1^2}{\gamma^2}\left[\frac{\gamma}{1-\gamma} + \ln(1-\gamma) - \frac{p^2}{1+\gamma} + p^2 - p^2\ln(1+\gamma)\right],$$

where

$$(3.19) \qquad \delta = \frac{b\varepsilon L^3}{2K_\theta G_0^3}.$$

Parameter θ_{Max} is the critical rotation angle in which the micromirror plate touches the electrodes plate and it is defined as

$$(3.20) \qquad \theta_{\mathrm{Max}} \cong \sin\theta_{\mathrm{Max}} = \frac{G_0}{L}.$$

At the equilibrium position, the electrostatic torque and the mechanical elastic torque are equal, meanwhile

$$(3.21) \qquad f(\gamma, p, \delta) = 0.$$

The rotation angle of the micromirror can be obtained by solving the nonlinear Eq. (3.21) at a specific applied voltage. For sufficiently low voltages, there are two physical exhibits of the rotation angle, where only one of them is stable. For a certain voltage, the two solutions of Eq. (3.21) coincide and pull-in phenomenon occurs. For voltages above the pull-in voltage, the electrostatic torque is greater than the mechanical torque for any angle [17].

By using the implicit function theorem and Eq. (3.21) to reach the maximum value of the $p(\gamma, \delta)$, the following equation should be satisfied:

$$(3.22) \qquad \frac{\partial f(\gamma, p, \delta)}{\partial \gamma} = 0.$$

Solving Eqs. (3.21) and (3.22) simultaneously, the pull-in parameters, pull-in voltage ($V_{\text{pull-in}}$) and angle of rotation (γ) of micromirror can be calculated.

4. Numerical solution

Stability analysis is conducted based on Eq. (3.18). For this purpose, we define the following phase space variables. AZIZI *et al.* [25] used this method for plotting bifurcation diagram and phase portrait of the electrostatically actuated microbeam

$$(4.1) \qquad \left\{ \begin{array}{c} S_1 \\ S_2 \end{array} \right\} = \left\{ \begin{array}{c} \gamma \\ \dot{\gamma} \end{array} \right\},$$

where S_1 and S_2 are the phase space variables and $\dot{\gamma}$ is the first derivative of γ with respect to time. The non-autonomous equation (3.18) reduces to the following so-called autonomous first-order differential equations:

$$\dot{S}_1 = F_1 = S_2,$$

$$(4.2) \qquad \begin{aligned} \dot{S}_2 &= F_2(S_1, S_2) \\ &= \frac{\delta V_1^2}{S_1^2} \left[\frac{S_1}{1 - S_1} + \ln(1 - S_1) - \frac{p^2}{1 + S_1} + p^2 - p^2 \ln(1 + S_1) \right] - \mu_\theta S_2 - S_1. \end{aligned}$$

The equilibrium points are found by setting the right-hand side of Eq. (24) equal to zero.

Assuming $\mu_\theta = 0$, it can be shown that the types of the equilibrium points of the system directly depend on the applied electrostatic voltages as follows:

$$S_1^* = S_2^* = 0,$$

$$S_2^* = 0,$$

(4.3)
$$\frac{1}{\sqrt{\dfrac{\delta}{S_1^*3}\left[\dfrac{S_1^*}{1-S_1^*} + \ln(1-S_1^*) - \dfrac{p^2}{1+S_1^*} + p^2 - p^2\ln(1+S_1^*)\right]}} = V_1,$$

where S_1^* and S_2^* correspond to the equilibrium positions.

5. Results and discussions

5.1. Validation

This section deals with the validation of the proposed numerical method. To this end, obtained pull-in voltages for a microactuator are compared with those obtained by Rezazadeh et al. [19] and Huang et al. [26]. The considered case study for this validation is a micromirror with thickness 1.5 μm, width 100 μm, shear modulus 66 GPa and initial gaps of $G_0 = 2.75$ μm. Here we must mention that in this paper, in contrast to Rezazadeh and Huang, we assumed that the distance between the axis of rotation and the edge of the electrode is equal to zero. The results of this comparison are shown in Table 1.

Table 1. Comparison between calculated results with those obtained by Rezazadeh *et al.* and Huang *et al.* at the pull-in point (saddle-node bifurcation).

Pull-in characteristics	Normalized rotation angle (γ)	V (V)
Experimental results (Huang et al.)	0.4198	17.4
Calculated results (Rezazadeh et al.)	0.5187	18.8
Calculated results	0.4404	16.21

The results of this comparison are in good agreements with those reported. This corresponding static pull-in voltage well agrees with the results of the static pull-in studies.

5.2. Saddle-node bifurcation ($p = 0$)

The geometrical and mechanical properties of the case study are presented in Table 2.

Table 2. Parameters of the electrostatic micromirror.

Items	Parameters	Values
Material properties	Shear modulus (Gpa)	66
Micromirror	Width $2L$ (μm)	100
	Length b (μm)	100
Torsion beam	Length l (μm)	65
	Width $2L$ (μm)	1.55
Electrode	Thickness t (μm)	1.5
	Coefficient c_2	0.1406
	Width L (μm)	50
	Initial gap G_0 (μm)	2.75

FIG. 4. Position and types of the fixed points versus applied voltage (bifurcation diagram).

When the voltages ratio is equal to zero, saddle-node bifurcation occurs. As shown in Fig. 4 for the given voltage V_1 $(0 < V_1 < V_{\text{pull-in}})$ there exist two fixed points, but for $V_1 > V_{\text{pull-in}}$ there is no fixed point. In order to check local stability in the vicinity of each fixed point, matrix A is defined as below:

$$(5.1) \qquad A = \begin{vmatrix} \dfrac{\partial F_1}{\partial S_1} & \dfrac{\partial F_1}{\partial S_2} \\ \dfrac{\partial F_2}{\partial S_1} & \dfrac{\partial F_2}{\partial S_2} \end{vmatrix} = 0.$$

The Jacobian of Eq. (5.1) is determined as [14]

$$(5.2) \qquad |A - \lambda I| = 0, \qquad \begin{vmatrix} -\lambda & 1 \\ \dfrac{\partial F_2(S_1, S_2)}{\partial S_1} & -\mu - \lambda \end{vmatrix} = 0.$$
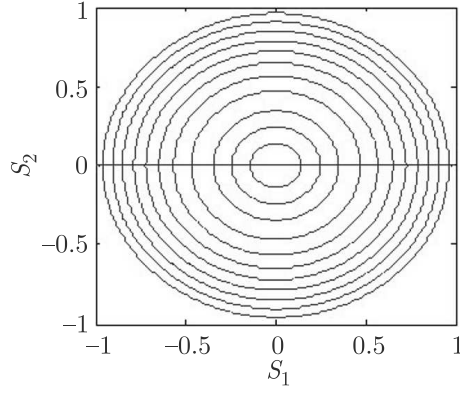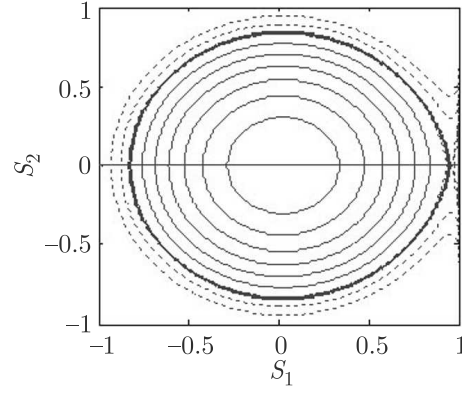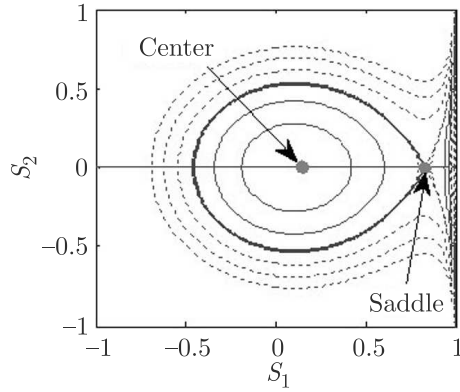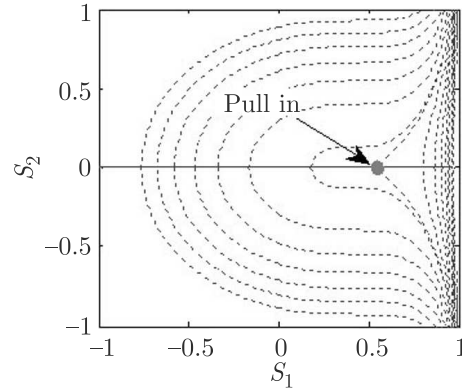
Equation (5.2) yields a characteristic equation for λ, in which the solution at each fixed point indicates the stability of that point. In the case without damping, the solution of the characteristic equation is simplified to

$$(5.3) \qquad\qquad \lambda_{1,2} = \pm\sqrt{\frac{\partial F_2(S_1, S_2)}{\partial S_1}}.$$

For $\lambda_{1,2} < 0$, it has two pure imaginary roots, which means that the fixed point is a center point. Applying the same method to other fixed points, its eigenvalues satisfy $\lambda_{1,2} > 0$, then it has two real eigenvalues, one is positive, and the other is negative. This means that the fixed point is an unstable saddle point [27, 28]. Using this method, the local stability in the vicinity of each fixed point in Fig. 4 can be identified. In this figure, continuous and dashed curves represent stable and unstable branches, respectively. As shown in Fig. 4, by increasing the controlling parameter V_1, distance between two fixed points is decreased and for $V_1 = 16.21$ V, they meet together in a saddle-node bifurcation, which is called "pull-in voltage" in the MEMS literature. Saddle-node bifurcation is a locally stationary bifurcation and can be analyzed based on locally defined eigenvalues. At bifurcation points associated with saddle-node bifurcation only branches of fixed points or static solutions meet. Hence, this bifurcation is classified as static bifurcations [29]. This type of bifurcation indicates qualitative change in a number of fixed points, in which an unstable and a stable branch meet together at the same point in the state-control space [30]. As shown in Fig. 4, the number of fixed points is decreased from two to zero points. The other name of this bifurcation is tangent bifurcation because tangencies of stable and unstable branches are the same at this point [29].

Figures 5–8 present free dynamic motion trajectories of the torsional micromirror for different values of the applied voltage V_1, with different initial conditions. As shown in Fig. 5 the response of the torsional micromirror for any initial condition is periodic when the applied voltage V_1 is considered zero. As shown in Fig. 5, origin is a stable center point and with any initial condition the response is periodic.

Figures 6 and 7 show motion trajectories of the actuator with applied voltages $V_1 = 5.4$ V and $V_1 = 10.8$ V, respectively. As shown in these figures, there are one center and one saddle point in each figure. Furthermore, there is a homoclinic orbit (bold-blue curves) in each figure. Homoclinic orbit originates in a saddle point and gets to this point [27, 31]. This orbit separates periodic region of a center point from unstable region of a saddle point [30]. When comparing two figures, it can be concluded that with increasing the applied voltage, the homoclinic orbit is contracted. Figure 8 illustrates motion trajectory of the micromirror with applied voltage $V_1 = 16.21$ V (pull-in voltage). As shown in

FIG 5. Phase portrait with given $V_1 = 0$ V.

FIG. 6. Phase portrait with given $V_1 = 5.4$ V.

FIG. 7. Phase portrait with given $V_1 = 10.8$ V.

FIG. 8. Phase portrait with given $V_1 = 16.21$ V.

this figure, homoclinic orbit disappears and the center and saddle points co-alesce and change to one saddle point. This phenomenon shows saddle-node bifurcation in global view of nonlinear dynamics. As shown in Fig. 8, structure is unstable for any initial condition.

5.3. Pitchfork bifurcation ($p = 1$)

Pitchfork bifurcation can be observed in the micromirror, when the applied voltages V_1 and V_2 are equal to each other. Figure 9 shows position of the fixed points versus applied voltage for $p = 1$. As shown in this figure by increasing the applied voltage V_1 as the control parameter three fixed points (two saddle points and a center point) are closed together and for $V_1 = 21.82$ V or pull-in voltage, they coalesce and change to one unstable saddle-node. As shown in this figure, $x = 0$ is a center point for $V_1 < 21.82$ V and it is a saddle point
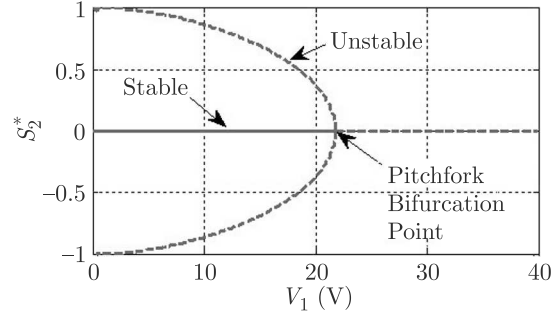
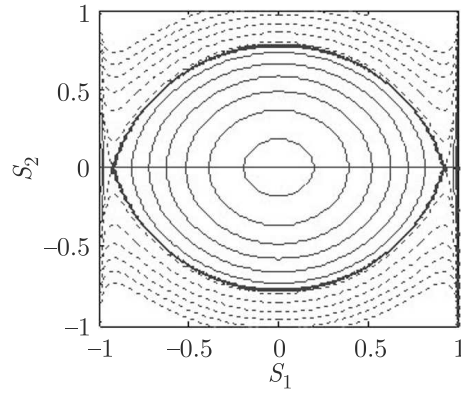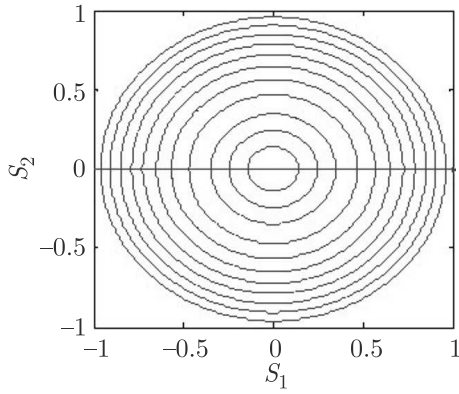Fig. 9. Position and types of the fixed points versus applied voltage (bifurcation diagram).

Fig 10. Phase portrait with given $V_1 = 0$ V.   Fig. 11. Phase portrait with given $V_1 = 7.27$ V.
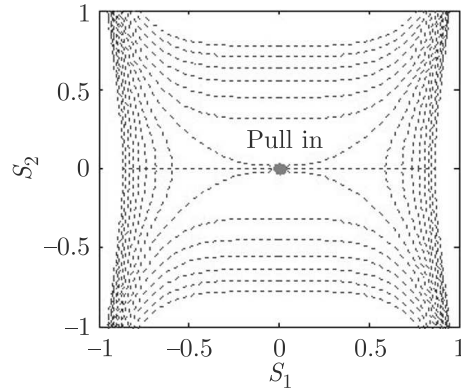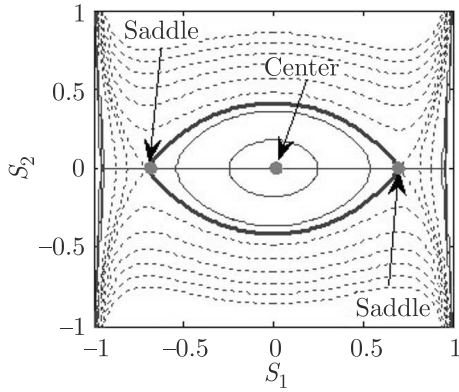

Fig. 12. Phase portrait with given $V_1 = 14.54$ V.   Fig. 13. Phase portrait with given $V_1 = 21.82$ V.

for $V_1 > 21.82$ V. This condition represents occurrence of a subcritical pitchfork bifurcation at $V_1 = 21.82$ V for the micromirror.

Figures 10–13 present the motion trajectories of the micromirror for different values of the applied voltage V_1 with different initial conditions. Figure 10 shows that the response of the torsional micromirror for any initial condition is periodic when the applied voltage is equal to zero. Figures 11 and 12 show phase portrait of the micromirror when the applied voltages are $V_1 = 7.27$ V and $V_1 = 14.54$ V, respectively. As shown in these figures, there are one center and two saddle points in each figure. Furthermore, there is a heteroclinic orbit (bold-blue curves) in each figure, which separates periodic solutions from the unbounded non-periodic solutions. A heteroclinic orbit may join a saddle-node to another one and may also join a saddle to a node, or vice versa [31]. Inside the heteroclinic orbit there is a connected series of periodic orbits whose periods increase monotonically and approach infinity as the heteroclinic orbit is approached [29]. As shown in these figures heteroclinic orbits are contracted with increasing the applied voltages.

Figure 13 illustrates motion trajectory of the micromirror for the applied voltage $V_1 = 21.82$ V (pull-in voltage). As shown in this figure heteroclinic orbit and periodic region disappeared. This condition occurs due to a collision of two saddle points with center point, which represents pitchfork bifurcation in the phase space as shown in Fig. 9.

5.4. Numerical results

To get the pull-in parameters, we also set $d^2\gamma/d\tau^2 = 0$ and $d\gamma/d\tau = 0$. The pull-in parameters are obtained as

$$
\begin{aligned}
&\gamma_{\text{pull−in}} = 0.4404, & V_{\text{pull−in}} = 16.21 \text{ V} \quad \text{(saddle node bifurcation)}, \\
&\gamma_{\text{pull−in}} = 0, & V_{\text{pull−in}} = 21.82 \text{ V} \quad \text{(pitchfork bifurcation)}.
\end{aligned}
\tag{5.4}
$$

However, the values of critical tilting angle and pull-in voltage are in fact dependent on the sizes of structures [18]. Here, 0.4404 is a universal constant for all electrostatically actuated torsional micromirrors. The pull-in effect is influenced by the dimensions of the electrode. This demonstrates again that "the electrodes determine the behavior of a torsional micromirror" [27, 31]. These values indicate obviously how to obtain a pull-in angle by selecting the electrode size, which is completely useful for the design of torsional micromirrors.

The numerical results about different configurations of the torsional micromirror are shown graphically in Figs. 14–19.
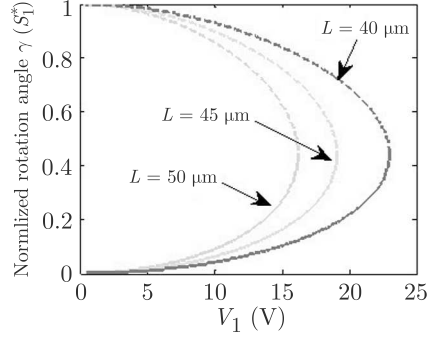
Fig. 14. The torsion angle versus the applied
voltage for different electrode sizes considering
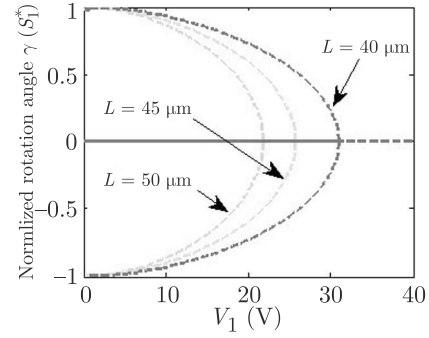the torsion effect (saddle-node bifurcation).

Fig. 15. The torsion angle versus the applied
voltage for different electrode sizes considering
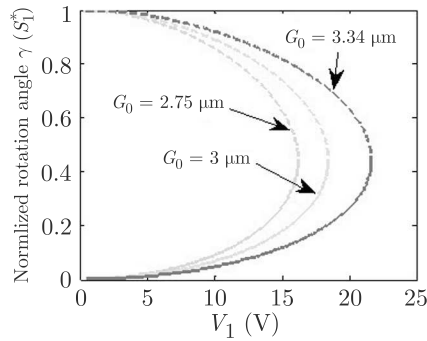the torsion effect (pitchfork bifurcation).

Fig. 16. The torsion angle versus the applied
voltage for different gap sizes considering
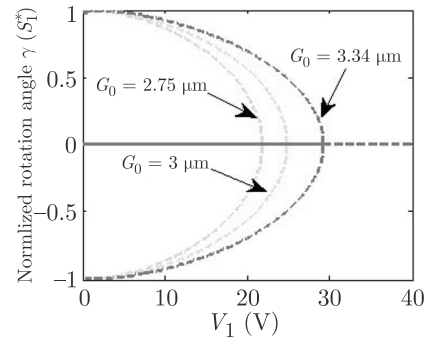the torsion effect (saddle-node bifurcation).

Fig. 17. The torsion angle versus the applied
voltage for different gap sizes considering
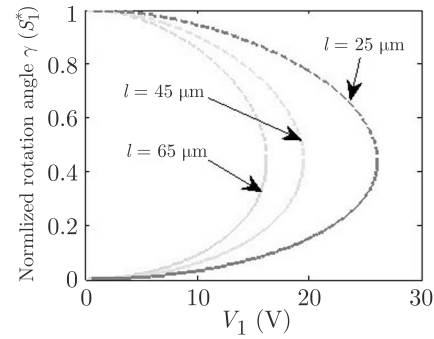the torsion effect (pitchfork bifurcation).

Fig. 18. The torsion angle versus the applied
voltage for different beam length sizes considering
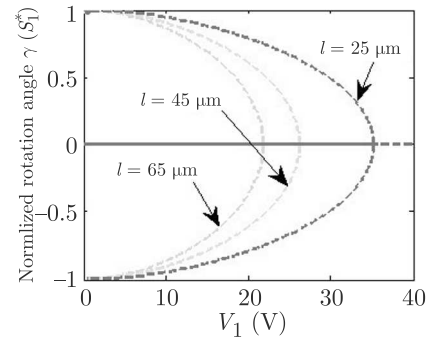the torsion effect (saddle-node bifurcation).

Fig. 19. The torsion angle versus the applied
voltage for different beam length sizes considering
the torsion effect (pitchfork bifurcation).

6. Conclusion

The nonlinear behavior of a torsional micromirror exposed to electrostatic actuation was studied. Next, the governing nonlinear equations were solved. The pull-in phenomena for the micro-actuator under various gap, electrode size and beam length were obtained and presented. The equation that governs the statics of the torsional micromirror was derived and the relationship between rotation angle and the driving voltage was determined.

By solving the equation of the static deflection, fixed points or equilibrium positions of the micromirror, when the voltage ratios are equal to zero ($p = 0$) and when the voltage ratios are equal to one ($p = 1$), are determined. Phase portraits and regions of bounded and unbounded solutions were illustrated. The nonlinear motion trajectories were shown in phase planes for various applied voltages and for different initial conditions.

It was shown that increase of the applied voltage leads the structure to an unstable condition by undergoing to saddle-node bifurcation in the case of $p = 0$, whereas in the case of $p = 1$ instability occurs when the structure undergoes a pitchfork bifurcation.

Acknowledgment

References

1. M. Bao, H. Yang, H. Yin, S. Shen, *Effects of electrostatic forces generated by the driving signal on capacitive sensing devices*, Sensors and Actuators A: Physical, **84**, 3, 213–219, 2000.

2. S. Lee, R. Ramadoss, M. Buck, V.M. Bright, K.C. Gupta, Y.C. Lee, *Reliability testing of flexible printed circuit-based RF MEMS capacitive switches*, Microelectronics Reliability, **44**, 2, 245–250, 2004.

3. T. Sasayama, S. Suzuki, S. Tsuchitani, A. Koide, M. Suzuki, T. Nakazawa, N. Ichikawa, *Highly reliable silicon micromachined physical sensors in mass production*, Sensors and Actuators A: Physical, **54**, 1–3, 714–717, 1996.

4. R. Sattler, F. Plötz, G. Fattinger, G. Wachutka, *Modeling of an electrostatic torsional actuator: demonstrated with an RF MEMS switch*, Sensors and Actuators A: Physical, **97–98**, 337–346, 2002.

5. C.F.R. Mateus, C. Chih-Hao, C.J. Chang-Hasnain, S. Yang, D. Sun, R. Pathak, *Tunable micromechanical optical filter using a torsional structure*, [in:] Optical Fiber Communication Conference and Exhibit, 2002, OFC 2002, 2002.

6. P.T. SAVADKOOHI, S. COLPO, B. MARGESIN, *Novel design of a RF-MEMS tuneable capacitor based on electrostatically induced torsion*, [in:] Design, Test, Integration & Packaging of MEMS/MOEMS, 2009, MEMS/MOEMS'09. Symposium on, 2009.

7. K. SLAVA, D.I. BARNEA, *Bouncing mode electrostatically actuated scanning micromirror for video applications*, Smart Materials and Structures, **14**, 6, 1281, 2005.

8. F. KHATAMI, G. REZAZADEH, *Dynamic response of a torsional micromirror to electrostatic force and mechanical shock*, Microsystem Technologies,**15**, 4, 535–545, 2009.

9. X.M. ZHANG, F.S. CHAU, C. QUAN, Y.L. LAM, A.Q. LIU, *A study of the static characteristics of a torsional micromirror*, Sensors and Actuators A: Physical, **90**, 1–2, 73–81, 2001.

10. L.J. HORNBECK, *128∗128 deformable mirror device*, Electron Devices, IEEE Transactions on, **30**, 5, 539–545, 1983.

11. T.-H. LIN, *Implementation and characterization of a flexure-beam micromechanical spatial light modulator*, Optical Engineering, **33**, 11, 3643–3648, 1994.

12. R.S. MULLER, K.Y. LAU, *Surface-micromachined microoptical elements and systems*, [in:] Proceedings of the IEEE, **86**, 8, 1705–1720, 1998.

13. J.M. YOUNSE, *Mirrors on a chip*, Spectrum, IEEE , **30**, 11, 27–31, 1993.

14. M. YOUNIS, *MEMS Linear and nonlinear statics and dynamics*, 1st ed., Springer, 2011.

15. M.I. YOUNIS, F. ALSALEEM, D. JORDY, *The response of clamped–clamped microbeams under mechanical shock*, International Journal of Non-Linear Mechanics, **42**, 4, 643–657, 2007.

16. J.-G. GUO, L.-J. ZHOU, Y.-P. ZHAO, *Instability analysis of torsional MEMS/NEMS actuators under capillary force*, Journal of Colloid and Interface Science, **331**, 2, 458–462, 2009.

17. O. DEGANI, E. SOCHER, A. LIPSON, T. LEJTNER, D.J. SETTER, S. KALDOR, Y. NEMIROVSKY, *Pull-in study of an electrostatic torsion microactuator*, Journal of Microelectromechanical Systems, **7**, 4, 373–379, 1998.

18. G. JIAN-GANG, Y.-P. ZHAO, *Influence of van der Waals and Casimir forces on electrostatic torsional actuators*, Journal of Microelectromechanical Systems, **13**, 6, 1027–1035, 2004.

19. G. REZAZADEH, F. KHATAMI, A. TAHMASEBI, *Investigation of the torsion and bending effects on static stability of electrostatic torsional micromirrors*, Microsystem Technologies, **13**, 7, 715–722, 2007.

20. W.H. LIN, Y.P. ZHAO, *Stability and bifurcation behaviour of electrostatic torsional NEMS varactor influenced by dispersion forces*, Journal of Physics D: Applied Physics, **40**, 6, 1649–1654, 2007.

21. W.H. LIN, Y.P. ZHAO, *Casimir effect on the pull-in parameters of nanometer switches*, Microsystem Technologies, **11**, 2–3, 80–85, 2005.

22. J. PING ZHAO, H. LING CHEN, J. MING HUANG, A. QUN LIU, *A study of dynamic characteristics and simulation of MEMS torsional micromirrors*, Sensors and Actuators A: Physical, **120**, 1, 199–210, 2005.

23. S.P. Timoshenko, J.N. Goodier, *Theory of Elasticity*, 3rd ed., McGraw-Hill Education, 1970.

24. W.-H. Lin, Y.-P. Zhao, *Influence of damping on the dynamical behavior of the electrostatic parallel-plate and torsional actuators with intermolecular forces*, Sensors, **7**, 12, 3012–3026, 2007.

25. S. Azizi, M.-R. Ghazavi, S. Esmaeilzadeh Khadem, G. Rezazadeh, C. Cetinkaya, *Application of piezoelectric actuation to regularize the chaotic response of an electrostatically actuated micro-beam*, Nonlinear Dynamics, 1–15, 2013.

26. J.M. Huang, A.Q. Liu, Z.L. Deng, Q.X. Zhang, J. Ahn, A. Asundi, *An approach to the coupling effect between torsion and bending for electrostatic torsional micromirrors*, Sensors and Actuators A: Physical, **115**, 1, 159–167, 2004.

27. W.-H. Lin, Y.-P. Zhao, *Nonlinear behavior for nanoscale electrostatic actuators with Casimir force*, Chaos, Solitons & Fractals, **23**, 5, 1777–1785, 2005.

28. J.-G. Guo, Y.-P. Zhao, *Dynamic stability of electrostatic torsional actuators with van der Waals effect*, International Journal of Solids and Structures, **43**, 3–4, 675–685, 2006.

29. A.H. Nayfeh, B. Balachandran, *Applied Nonlinear Dynamics*, Wiley, 2004.

30. H. Mobki, G. Rezazadeh, M. Sadeghi, F. Vakili-Tahami, M.-M. Seyyed-Fakhrabadi, *A comprehensive study of stability in an electro-statically actuated micro-beam*, International Journal of Non-Linear Mechanics, **48**, 78–85, 2013.

31. R. Seydel, *Practical Bifurcation and Stability Analysis*, 3rd ed., Springer, 2010.